

Spectral and Steady-State Properties of Random Liouvillians

Lucas Sá,^{1,*} Pedro Ribeiro,^{1,2,†} and Tomaž Prosen^{3,‡}

¹*CeFEMA, Instituto Superior Técnico, Universidade de Lisboa, Av. Rovisco Pais, 1049-001 Lisboa, Portugal*

²*Beijing Computational Science Research Center, Beijing 100193, China*

³*Department of Physics, Faculty of Mathematics and Physics, University of Ljubljana, Ljubljana, Slovenia*

We study generic open quantum systems with Markovian dissipation, focusing on a class of stochastic Liouvillian operators of Lindblad form with independent random dissipation channels (jump operators) and a random Hamiltonian. We establish that the global spectral features, the spectral gap, and the steady-state properties follow three different regimes as a function of the dissipation strength, whose boundaries depend on the particular observable. Within each regime, we determine the scaling exponents with the dissipation strength and system size. We find that, for two or more dissipation channels, the spectral gap increases with the system size. The spectral distribution of the steady-state is Poissonian at low dissipation strength and conforms to that of a random matrix once the dissipation is sufficiently strong. Our results can help to understand the long-time dynamics and steady-state properties of generic dissipative systems.

An open quantum system is strongly influenced by its environment. However, a complete description of how the degrees of freedom of a system and its environment evolve is impractical and often impossible. One of the simplest ways to model open quantum dynamics is by using an effective master equation, $\partial_t \rho = \mathcal{L}(\rho)$, to describe the evolution of the system's reduced density matrix, where the Liouvillian acquires the Lindblad form [1]

$$\mathcal{L} = \mathcal{L}_H + \sum_{\ell} \mathcal{D}_{W_{\ell}}, \quad (1)$$

with $\mathcal{L}_H(\rho) = -i[H, \rho]$ representing the unitary evolution under the Hamiltonian H , and $\mathcal{D}_{W_{\ell}}(\rho) = W_{\ell} \rho W_{\ell}^{\dagger} - \frac{1}{2} W_{\ell}^{\dagger} W_{\ell} \rho - \frac{1}{2} \rho W_{\ell}^{\dagger} W_{\ell}$ the contribution of each dissipation channel by the action of the jump operator W_{ℓ} . This approach assumes a weakly coupled environment with memory times much shorter than all other characteristic energy scales. Due to this so-called Markovian assumption, Lindblad dynamics fails to capture certain processes, such as the ones responsible for coherent low temperature transport [2]. Nevertheless, the method is widely used in areas ranging from thermodynamics of quantum engines [3] to the description of quark-gluon plasma [4]. Perhaps, its most important application is to model quantum optic setups, which typically fulfill the required conditions as driving fields shift the relevant energies of the environment to a region where the spectral density is large [5].

Although the Lindblad form significantly simplifies the problem, obtaining dynamic and steady-state properties given a Lindblad operator remains a major theoretical challenge. In one dimension, efficient numerical approaches have been developed based on matrix product operator ideas [6, 7]. An alternative strategy, that has recently been extremely successful, consists of studying exactly solvable (or integrable) models [8–13]. Although enlightening, integrable Lindbladians, as their Hamiltonian counterparts, are expected to have very peculiar properties and remain a set of zero-measure among all

possible Lindbladian dynamics. In the general case, one has to rely on exact diagonalization which remains restricted to relatively small systems.

For non-integrable closed quantum systems, systematic tools are also available to study fully chaotic Hamiltonians. They rely on the widely supported conjecture [14] which asserts that universal features of spectral and eigenstate properties of quantum systems with a well defined chaotic classical limit follow those of random matrix theory (RMT). This is to be contrasted with integrable systems where level spacings typically follow Poisson statistics. RMT has been also reported to predict complex many-body systems without well defined classical correspondents. These predictions are particularly appealing as they are insensitive to the microscopic details of particular models, relying solely on symmetry properties of the Hamiltonian, i.e. to which: Gaussian unitary (GUE), Gaussian orthogonal (GOE), or Gaussian symplectic (GSE) ensemble, it belongs to. In view of the tremendous success of RMT it is natural to ask if a similar approach can be followed in the case of Lindbladian dynamics. This route has, however, remained essentially unexplored up to very recently [15–17].

Following these general ideas, Ref. [15] studies an ensemble of random Lindblad operators with a maximal number of independent decay channels and finds that in this case the spectrum acquires an universal lemon-shaped form. In a similar spirit, Ref. [16] considers an ensemble of random Lindbladians consisting of a Hamiltonian part and a finite number of Hermitian jump operators and finds a sharp spectral transition as a function of the dissipation strength. Finally, Ref. [17] studies in detail the spectral gap for several different Liouvillians. Yet, there are a number of open questions related to the nature of the spectrum, specifically when the dissipative and the Hamiltonian components are comparable. Additionally, the properties of the non-trivial steady-state, ensuing in the presence of non-Hermitian jump operators, are completely unexplored.

The aim of this Letter is to study the universal properties of the spectrum and the steady-state of Liouvillian operators consisting of an Hamiltonian component and a set of dissipation channels, taken from appropriate ensembles of random matrices. We consider a finite number of non-Hermitian jump operators allowing for a non-trivial steady-state. As a function of the effective dissipation strength, g_{eff} , we find a rich set of regimes regarding global spectral features such as the spreading of the decay rates X , the spectral gap Δ , and the spectral properties of the steady-state density matrix ρ_0 . Each regime is characterized by a scaling of the corresponding quantity with the system size N and with g_{eff} . The finite-size scaling of the boundaries between different regimes was also determined. The paper is organized as follows. First, we describe an unbiased construction of a random Liouvillian. Second, we study its spectral and steady-state properties. Finally, we end with a short summary of our findings and their implications for determining properties of generic Markovian dissipative systems.

To obtain a suitable set of random Liouvillians of the Lindblad form, we define a complete orthogonal basis, $\{G_i\}$ with $i = 0, \dots, N^2 - 1$, for the space of operators acting on an Hilbert space of dimension N , respecting $\text{tr}[G_i^\dagger G_j] = \delta_{ij}$, with $G_0 = \frac{1}{\sqrt{N}}$ proportional to the identity. Each jump operator can be decomposed as $W_\ell = \sum_{j=1}^{N^2-1} G_j l_{j\ell}$. Note that W_ℓ is taken to be traceless, i.e. orthogonal to G_0 , to ensure that the dissipative term in Eq. (1) does not contribute to the Hamiltonian dynamics. In the $\{G_i\}$ basis, the Liouvillian is completely determined by matrices H and l ,

$$\mathcal{L}(\rho) = -i[H, \rho] + g^2 \sum_{j,k=1}^{N^2-1} d_{jk} \left\{ G_j \rho G_k^\dagger - \frac{1}{2} [\rho G_k^\dagger G_j + G_k^\dagger G_j \rho] \right\}, \quad (2)$$

where $d_{jk} = \sum_{\ell=1}^r l_{j\ell} l_{k\ell}^* = (ll^\dagger)_{jk}$ is an $N^2 - 1 \times N^2 - 1$ positive-definite matrix. We denote by r the number of jump operators in Eq. (1), i.e. $\ell = 1, \dots, r$. To obtain a random Liouvillian, we draw H from a Gaussian ensemble with unit variance, i.e. $P_N(H) \propto e^{-\frac{1}{2}\text{tr}(H^2)}$, and l from a Ginibre ensemble, $P_{(N^2-1, r)}(l) \propto e^{-\frac{1}{2}\text{tr}(l^\dagger l)}$. The coupling constant $g > 0$ parameterizes the dissipation strength. We consider two cases: real matrices, $H_{ij} = H_{ji}, l_{ij} \in \mathbb{R}$ (labeled by $\beta = 1$ in the following), and complex matrices, $H_{ij} = H_{ji}^*, l_{ij} \in \mathbb{C}$ ($\beta = 2$). We consider the statistical properties of the spectrum of \mathcal{L} drawn from an ensemble of random Lindblad operators parameterized by N , r , β and g . The right eigenvectors of \mathcal{L} , respecting $\mathcal{L}(\rho_\alpha) = \Lambda_\alpha \rho_\alpha$, with $\alpha = 0, \dots, N^2 - 1$, are denoted by ρ_α , with Λ_α the respective eigenvalue. By construction, $\text{Re}(\Lambda_\alpha) \leq \Lambda_0 = 0$, and ρ_0 , if unique, is the asymptotic steady-state, left invariant by the evolution. The spectrum and eigenvectors of \mathcal{L} are obtain by exact

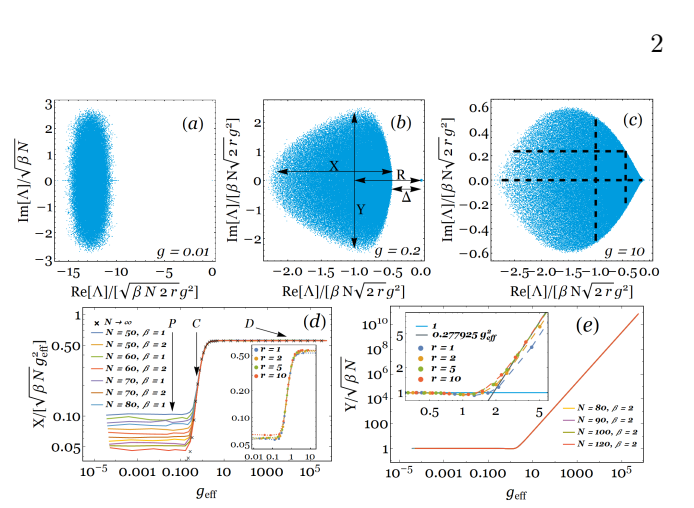


Figure 1. (a) – (c) Spectrum of a random Lindblad operator for different values of g , computed for $N = 80$, $\beta = 2$ and $r = 2$. R , X , Y and Δ are, respectively, the center for mass of the spectrum, the standard deviation along the real and imaginary axes, and the spectral gap. The horizontal (vertical) dashed lines in (c) correspond to 0 , Y (R , $R + X$). (d) and (e) show the scaling of X and Y for different values of N and r as a function of $g_{\text{eff}} = (2r\beta N)^{1/4} g$.

diagonalization.

Figs. 1 (a) to (c) show the spectrum of a random Lindblad operator in the complex plane computed for different values of g . Besides the spectral gap, $\Delta = \min_{\alpha > 0} \text{Re}(-\Lambda_\alpha)$, we also illustrate the center of mass of the spectrum, $R = \sum_{\alpha} \Lambda_\alpha / N^2$, and the variance along the real, $X^2 = \sum_{\alpha} [\text{Re}(\Lambda_\alpha - R)]^2 / N^2$, and imaginary, $Y^2 = \sum_{\alpha} (\text{Im}\Lambda_\alpha)^2 / N^2$, axes. The boundaries of the spectrum evolve from an ellipsoid, for small g , to a lemon-like shape at large g . These results, obtained here for $r = 2$, indicate that the lemon-shaped spectral boundary, found in Ref. [15] for the case $r = N^2 - 1$, is ubiquitous in the strong dissipation regime, although, contrarily to the $r = N^2 - 1$ case, the spectral distribution is not uniform within its support.

In the limit of large N , the center of mass is found to scale as $R \propto \beta N r g^2$ (not shown in the figure, see [18]). Figs. 1 (d) and (e) show the scaling of X and Y with N as a function of

$$g_{\text{eff}} = (2r\beta N)^{1/4} g. \quad (3)$$

The three representative points (P, C, D) of Fig. 1 (d) correspond to regimes for which X depicts a qualitative different behavior. The observed scaling collapse shows that, for large g_{eff} , the standard deviation along the real axis behaves as $X \propto [(\beta N)^{1/4} g_{\text{eff}}]^2 f_X^>(g_{\text{eff}})$, with $f_X^>$ an unknown scaling function satisfying $f_X^>(x) \propto x^0$ for $x \rightarrow \infty$ and $f_X^>(x) \propto x^2$ for $x \rightarrow 0$. A similar scaling collapse can be obtained for small g_{eff} (not shown, see [18]) yielding $X \simeq g_{\text{eff}}^2 f_X^<[(\beta N)^{1/4} g_{\text{eff}}]$, for which the scaling function satisfies $f_X^<(x) \propto x^0$ when $x \rightarrow 0$ and $f_X^<(x) \propto x^2$ when $g_{\text{eff}} \rightarrow \infty$. The asymptotic power

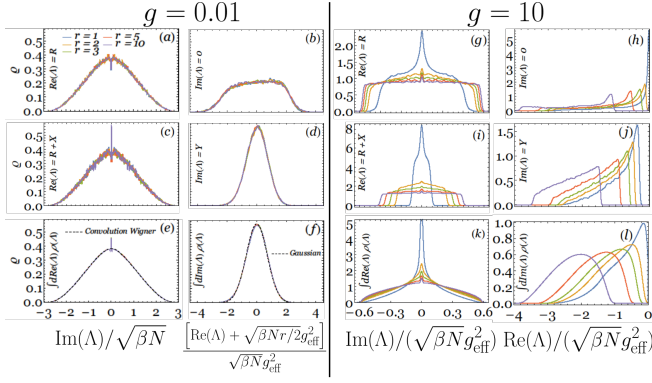


Figure 2. Spectral density along the cuts $\text{Re}(\Lambda) = R$, $R + X$ and $\text{Im}(\Lambda) = 0$, Y , computed for $N = 80$, $\beta = 2$, several values of r and two values of g , such that the system is in regime P: (a) – (d); and in regime D: (g) – (j). (e), (f): integrated density along the real and imaginary axes, $\varrho_{\text{I}}(\Lambda_{\text{I}})$ and $\varrho_{\text{R}}(\Lambda_{\text{R}})$, for regime P. In (b), (d) and (f) the zero eigenvalue is omitted. (k) and (l): same quantities for regime D.

law behavior of the scaling functions is hard to determine for the available values of $N \leq 120$, however, it is fully compatible with the large N extrapolation both in the large and small g_{eff} regimes (see black crosses in Fig. 1 (d) and [18]). This result is further corroborated by the compatibility conditions $\lim_{g_{\text{eff}} \rightarrow 0} (\beta N)^{1/2} f_X^>(g_{\text{eff}}) \simeq \lim_{(\beta N)^{1/4}, g_{\text{eff}} \rightarrow \infty} f_X^<[(\beta N)^{1/4} g_{\text{eff}}]$ (for further details see [18]). We can thus identify the three regimes: P, for $g_{\text{eff}} \lesssim (\beta N)^{-1/4}$; C, for $(\beta N)^{-1/4} \lesssim g_{\text{eff}} \lesssim (\beta N)^0$; and D, for $(\beta N)^0 \lesssim g_{\text{eff}}$, corresponding to each representative point. Note that the rescaled quantities plotted in Fig. 1 (d) and (e) do not seem to depend on the index β . There is a small r -dependence, which converges rapidly for increasing r (see insets). For the standard deviation along the imaginary axes we find, $Y \simeq \sqrt{\beta N}$ for regimes P and C, and $Y \propto \sqrt{\beta N} g_{\text{eff}}^2$ within regime D. Therefore, the variance in regime P can be explained by a perturbative treatment of the dissipative term - the value of Y corresponds to the unit variance of the random Hamiltonian, and $X \propto g_{\text{eff}}^2$ is expected from a degenerate perturbation theory.

Figs. 2 (a) to (f) and (g) to (l) show the spectral density, $\varrho(\Lambda) = \sum_{\alpha} \delta^2(\Lambda - \Lambda_{\alpha})$, along the cuts depicted in Figs. 1 (c) for regimes P and D, respectively, for various numbers of jump operators. Results for $\beta = 1$, i.e. real matrices, show the same limiting behavior in the large N limit, after proper rescaling. For P, the density along $\text{Re}(\Lambda) = R$ and $R + X$, does not depend on the number of jump operators, r . The integrated distribution of the imaginary parts, $\varrho_{\text{I}}(\Lambda_{\text{I}}) = \int d^2\Lambda \delta(\Lambda_{\text{I}} - \text{Im}\Lambda) \varrho(\Lambda)$, is well described by a convolution of Wigner's semicircle laws, $\varrho_{\text{W}}(E) \simeq \sqrt{E_*^2 - E^2}$, i.e. $\varrho_{\text{I}}(\Lambda_{\text{I}}) \simeq \int dE_1 dE_2 \delta(\Lambda_{\text{I}} - E_1 + E_2) \varrho_{\text{W}}(E_1) \varrho_{\text{W}}(E_2)$, except at $\Lambda_{\text{I}} = 0$ where there is an increase of spectral weight depleted from the immediate vicinity of this point. The

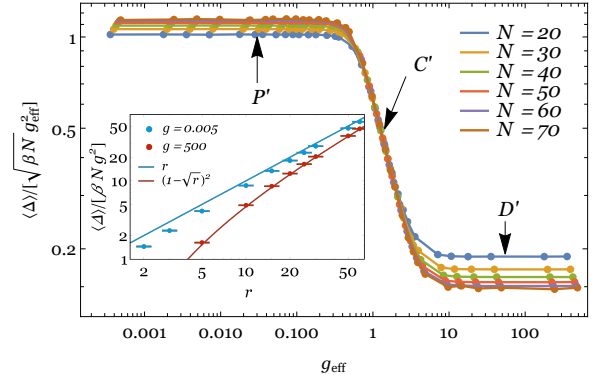


Figure 3. Average spectral gap as a function of g_{eff} plotted for different values of N for $\beta = 2$ and $r = 2$. Inset: evolution of the spectral gap with the number of jump operators r , for $N = 60$, $\beta = 1, 2$ and $g = 0.005$ (blue) and $g = 500$ (red); the full lines correspond to the analytic predictions.

spectral weights along the cuts $\text{Im}(\Lambda) = 0$ and Y scale with \sqrt{r} and the integrated distribution of the real parts, $\varrho_{\text{R}}(\Lambda_{\text{R}}) = \int d^2\Lambda \delta(\Lambda_{\text{R}} - \text{Re}\Lambda) \varrho(\Lambda)$, is well approximated by a Gaussian. As for the variance, in the P regime, these results can be derived from a perturbative small- g expansion. In the strong dissipative regime, D, the spectral density along $\text{Re}(\Lambda) = R$ and $R + X$, depends on r but converges rapidly to the $r \rightarrow \infty$ limit. The case $r = 1$ is qualitatively different from $r > 1$. This can also be observed in the $\text{Im}(\Lambda) = 0$ and Y cuts, and in ϱ_{R} , where for $r = 1$ the spectral weight is finite for $\Lambda_{\text{R}} \rightarrow 0^-$, in contrast with the $r > 1$ results that develop a spectral gap.

We now turn to the study of Δ , which is a particularly important spectral feature since it determines the long-time relaxation asymptotics. Figs. 3 shows the average spectral gap, $\langle \Delta \rangle$, for $\beta = 2$ and $r = 2$ as a function of g_{eff} for different values of N . In [18], we checked that in the thermodynamic limit the distribution of the gap becomes sharply peaked around its mean; hence, the latter accurately describes the long-time dynamics.

Here, we also find three qualitatively different regimes (P', C', D') whose boundaries *do not* coincide with those in Figs. 1. Here the boundaries $g_{\text{eff}} \simeq g_{\text{P}'\text{C}'}$ and $g_{\text{eff}} \simeq g_{\text{C}'\text{D}'}$, separating the P' and C', and the C' and D' regimes, respectively, are independent of N for $N \rightarrow \infty$. For regime P', the average gap behaves as $\langle \Delta \rangle \propto (\beta N)^{1/2} g_{\text{eff}}^2$; for C', the gap varies as $\langle \Delta \rangle \propto (\beta N)^{1/2} g_{\text{eff}}$; for D', we observe $\langle \Delta \rangle \propto (\beta N)^{1/2} g_{\text{eff}}^2$. As before, these results are only possible to establish by performing a large N extrapolation of the available data due to the presence of large finite size corrections [18].

The limiting $N \rightarrow \infty$ values of the spectral gap for small- and large- g_{eff} can be determined either by perturbative arguments or by computing the holomorphic Green's functions, respectively (see [18] for details). One finds that $\langle \Delta \rangle = \beta N g^2 (1 - \sqrt{r})^2$ for large g_{eff} , which is

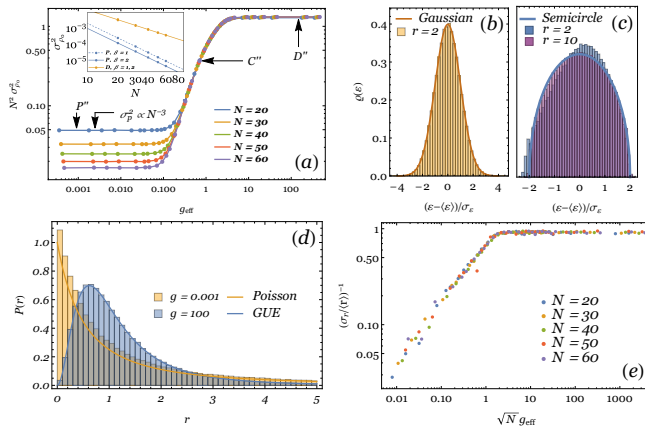


Figure 4. (a): Variance of steady-state probabilities as a function of g_{eff} plotted for different values of N for $\beta = 2$ and $r = 2$. (b)–(c): spectral density for the effective Hamiltonian \mathcal{H} for $g = 0.001$ and $g = 100$, respectively. (d): Statistics of level spacing ratios for weak and strong dissipation and comparison with approximate analytic predictions for Poisson and RMT statistics (solid lines). (e): ratio of the first two moments of the distribution of r , $(\sigma_r / \langle r \rangle)^{-1}$, for $\beta = 2$ and $r = 2$.

compatible with Ref. [17]. For small g_{eff} , employing degenerate perturbation theory to generalize the results of Ref. [19] (see [18]), we find that for large r the average gap is given by $\langle \Delta \rangle = \beta N g^2 r$. The predictions describe the gap increasingly well for growing r ; for $r = 2$, although not exact, they give a good estimate, see inset in Fig. 3. Notwithstanding that the above two results are derived in the limits $g_{\text{eff}} \rightarrow 0$ and $g_{\text{eff}} \rightarrow \infty$, they provide a remarkable description for the whole P' and D' regimes, respectively. For the special case $r = 1$, although three regimes are also present, see [18], the gap closes in the thermodynamic limit for large g_{eff} . Finally, none of the regimes above show the mid-gap states reported in [16], where only Hermitian jump operators were considered.

We now turn to the characterization of the steady-state ρ_0 . First, we consider the variance, $\sigma_{\rho_0}^2$, of the eigenvalues of ρ_0 . This quantity is related to the difference between the purity of the steady-state, $\mathcal{P}_0 = \text{tr}(\rho_0^2)$, which quantifies the degree of mixing of ρ_0 , and that of a fully-mixed state $\mathcal{P}_{\text{FM}} = 1/N$, $\mathcal{P}_0 - \mathcal{P}_{\text{FM}} = N \sigma_{\rho_0}^2$.

Fig. 4 (a) shows the variance $\sigma_{\rho_0}^2$ as a function of g_{eff} for $\beta = 2$ and $r = 2$. Here again, three different regimes can be observed whose boundaries *do not* coincide with those given for previous quantities. In regime P'', $g_{\text{eff}} \lesssim (\beta N)^{-1/2}$, we observe $\sigma_{\rho_0}^2 \propto N^{-3} f_{\rho_0}^<(N^{1/2} g_{\text{eff}})$, with $f_{\rho_0}^<(x) \propto x^0$, for $x \rightarrow 0$, and $f_{\rho_0}^<(x) \propto x^2$ for $x \rightarrow \infty$. In regime D'', for $N^0 \lesssim g_{\text{eff}}$, we have $\sigma_{\rho_0}^2 \propto N^{-2} f_{\rho_0}^>(g_{\text{eff}})$ (see inset), with $f_{\rho_0}^>(x) \propto x^0$ for $x \rightarrow \infty$ and $f_{\rho_0}^>(x) \propto x^2$ for $x \rightarrow 0$. The crossover regime C'' can be accessed by both asymptotic expansions and corresponds to $\sigma_{\rho_0}^2 \propto N^{-2} g_{\text{eff}}^2$. The asymptotic matching again agrees with data extrapolation, see [18]. These scalings imply that,

up to subleading $1/N$ corrections, the steady-state is fully mixed in regime P'', $\langle \mathcal{P}_0 \rangle = \mathcal{P}_{\text{FM}} + \mathcal{O}(1/N^2)$, while in regimes C'' and D'', \mathcal{P}_0 is only proportional to \mathcal{P}_{FM} . The case with $r = 1$ is again qualitatively different from $r > 1$ at strong dissipation, the purity $\langle \mathcal{P}_0 \rangle$ being of order N^0 (see [18]), signaling a steady-state closer to a pure state than a fully-mixed one.

Next, we investigate the steady-state's spectrum. For that, it is useful to introduce the effective Hamiltonian $\mathcal{H} = -\log \rho_0$. We denote the eigenvalues of \mathcal{H} by ε and present their spectral density $\varrho(\varepsilon)$ in Figs. 4 (b) and (c), corresponding to a point in regime P'' and D'', respectively. In the weak coupling regime, P'', $\varrho(\varepsilon)$ is well described by a Gaussian, while at strong coupling, D'', it acquires a non-Gaussian shape. For large r , $\varrho(\varepsilon)$ is increasingly well described by a Wigner semicircle distribution. A remarkable agreement can already be seen for $r = 10$ in the example of Fig. 4 (c). For small r (see $r = 2$ in the Fig. 4 (c)) there is a systematic skewing of the spectrum to the right.

Fig. 4 (d) presents the probability distribution, $P(r)$, of adjacent spacing ratios, $r_i = s_i / s_{i-1}$, with $s_i = \varepsilon_{i+1} - \varepsilon_i$, which automatically unfolds the spectrum of \mathcal{H} [20]. The analytic predictions for the GUE and for the Poisson distribution [20] (full lines) are given for comparison. The agreement of the numerical data of the points in the P'' and D'' regimes, respectively, with the Poisson and GUE predictions is remarkable. Within regime C'', we observe a crossover between these two regimes.

To illustrate the changing of the spectral properties of \mathcal{H} with g_{eff} , we provide in Fig. 4 (e) the ratio of the first two moments of the distribution of r , $(\sigma_r / \langle r \rangle)^{-1}$ which can distinguish between Poisson and GUE statistics. Since in the Poissonian case $P(r) = 1/(1+r)^2$, the n -th moment of the distribution diverges faster than the $(n-1)$ -th and thus $\sigma_r / \langle r \rangle \rightarrow \infty$. On the other hand, for GUE or GOE this ratio is given by a finite number of order unity (e.g. $\sigma_r / \langle r \rangle = 256\pi^2 / (27\sqrt{3} - 4\pi)^2 - 1 \simeq 1.160$ for GUE). Fig. 4 (e) shows that the Poissonian statistics are only attained in the dissipationless limit $N^{1/2} g_{\text{eff}} \rightarrow 0$. On the other hand, the GUE (for $\beta = 2$) or GOE (for $\beta = 1$) values are attained for $g_{\text{eff}} N^{1/2} \simeq 1$. Thus, in the thermodynamic limit the effective Hamiltonian \mathcal{H} is quantum chaotic for all finite values of g_{eff} .

In summary, by analyzing an ensemble of stochastic Liouvillians of Lindblad form, where unitary dynamics coexists with r independent dissipation channels, we find that the dispersion of the decay rates, the spectral gap and the properties of the steady-state are divided into different regimes, namely a regime of weak-dissipation, a crossover, and a strong dissipative regime. However, the boundaries of each regime do not necessarily coincide for the different observables. Each of the scaling regimes, as well as their boundaries, can be characterized by a set of exponents which rule the dependence of the observable on the effective dissipation strength, g_{eff} , and on the system

size N . We find that these exponents are independent from the universality index β of random matrices and determined their approximate scaling exponents.

As dissipation increases, the support of the spectrum passes from an ellipsoid to the lemon-like shape reported in Ref. [15] for the case of $r = N^2 - 1$. However, even in this regime, the distribution of eigenvalues only becomes homogeneous within its support for large values of r . For fixed g_{eff} and $r > 1$, the spectral gap increases with N and its distribution becomes peaked in the $N \rightarrow \infty$ limit. The case of a single dissipation channel, $r = 1$, is qualitatively different. For $r = 1$, Δ vanishes with increasing N in the strong dissipative regime. Finally, with increasing system size and $r > 1$, the steady-state purity approaches that of the maximally mixed state, $\mathcal{P}_{\text{FM}} = 1/N$, in the weak dissipative regime, while for strong dissipation it attains a value larger than, though proportional to, \mathcal{P}_{FM} . The steady-state spectral statistics exhibit a crossover from Poissonian to GUE (GOE) for $\beta = 2$ (1) as a function of $g_{\text{eff}}N^{1/2}$.

A natural question our results raise is—which regime characterizes a particular physical system? As in the case of chaotic Hamiltonian dynamics, this has to be determined on a case-by-case basis, which we will delegate to future works. The predictive power of the present analysis relies on the fact that, once this regime is determined, the system’s universal properties can be obtained solely by symmetry arguments.

PR acknowledges support by FCT through the Investigador FCT contract IF/00347/2014 and Grant No. UID/CTM/04540/2013. TP acknowledges ERC Advanced grant 694544-OMNES and ARRS research program P1-0402.

* lucas.seara.sa@tecnico.ulisboa.pt

† ribeiro.pedro@gmail.com

‡ tomaz.prosen@fmf.uni-lj.si

- [1] H.-P. Breuer and F. Petruccione, *The Theory of Open Quantum Systems* (Oxford University Press, 2002).
- [2] P. Ribeiro and V. R. Vieira, *Physical Review B* **92**, 100302 (2015), [arXiv:1412.8486](https://arxiv.org/abs/1412.8486).
- [3] P. P. Hofer, M. Perarnau-Llobet, L. D. M. Miranda, G. Haack, R. Silva, J. B. Brask, and N. Brunner, *New Journal of Physics* **19**, 123037 (2017).
- [4] D. D. Boni, *Journal of High Energy Physics* **2017** (2017), [10.1007/jhep08\(2017\)064](https://arxiv.org/abs/10.1007/jhep08(2017)064).
- [5] C. Gardiner and P. Zoller, *Quantum noise: a handbook of Markovian and non-Markovian quantum stochastic methods with applications to quantum optics*, Vol. 56 (Springer Science & Business Media, 2004).
- [6] F. Verstraete, J. J. García-Ripoll, and J. I. Cirac, *Physical Review Letters* **93** (2004), [10.1103/physrevlett.93.207204](https://arxiv.org/abs/10.1103/physrevlett.93.207204).
- [7] T. Prosen and M. Žnidarič, *Journal of Statistical Mechanics: Theory and Experiment* **2009**, P02035 (2009).
- [8] T. Prosen, *New Journal of Physics* **10**, 043026 (2008).

- [9] T. Prosen, *Physical Review Letters* **107**, 137201 (2011), [arXiv:1106.2978](https://arxiv.org/abs/1106.2978).
- [10] T. Prosen, *Physical Review Letters* **112**, 030603 (2014).
- [11] M. V. Medvedyeva, F. H. L. Essler, and T. Prosen, *Physical Review Letters* **117**, 137202 (2016).
- [12] D. A. Rowlands and A. Lamacraft, *Physical Review Letters* **120**, 090401 (2018).
- [13] P. Ribeiro and T. Prosen, *Physical Review Letters* **122** (2019), [10.1103/physrevlett.122.010401](https://arxiv.org/abs/10.1103/physrevlett.122.010401).
- [14] O. Bohigas, M. J. Giannoni, and C. Schmit, *Physical Review Letters* **52**, 1 (1984).
- [15] S. Denisov, T. Lapyteva, W. Tarnowski, D. Chruściński, and K. Życzkowski, [arXiv:1811.12282](https://arxiv.org/abs/1811.12282) (2018).
- [16] T. Can, V. Oganesyan, D. Orgad, and S. Gopalakrishnan, [arXiv:1902.01414](https://arxiv.org/abs/1902.01414) (2019).
- [17] T. Can, [arXiv:1902.01442](https://arxiv.org/abs/1902.01442) (2019).
- [18] See Supplemental Material for further numerical details, results for $r=1$ and an analytic analysis on limiting values of spectral quantities, which includes Refs. [21–24].
- [19] C. Timm, *Physical Review E* **80**, 021140 (2009).
- [20] Y. Atas, E. Bogomolny, O. Giraud, and G. Roux, *Physical Review Letters* **110**, 084101 (2013).
- [21] F. Haake, *Quantum signatures of chaos*, Vol. 54 (Springer Science & Business Media, 2013).
- [22] J. Feinberg and A. Zee, *Nuclear Physics B* **504**, 579 (1997).
- [23] J. Jurkiewicz, G. Łukaszewski, and M. A. Nowak, *Acta Physica Polonica B* **39** (2008).
- [24] J. Ståring, B. Mehlig, Y. V. Fyodorov, and J. Luck, *Physical Review E* **67**, 047101 (2003).

Supplementary Material: Spectral and Steady-State Properties of Random Liouvillians

In the Supplementary Material we provide a summary of the various scaling exponents (for scaling with N and g_{eff}) for $r > 1$ (given in the main text for $r = 2$) and for $r = 1$ (Sec. S1). We also give further details for the evolution of global spectral properties (Sec. S2), the spectral gap (Sec. S3) and steady-state properties (Sec. S4) for $r > 1$ and compare with the results for $r = 1$ (Sec. S5).

S1. Summary of exponents

The compatibility of scaling arguments given in the main text for X and $\sigma_{\rho_0}^2$ can be given in general, for any quantity which has the same qualitative behaviour as the ones described in this work. This procedure also allows us to systematize the exponents found in the main text, by defining three types of exponents: ν , κ and λ , related to the finite-size scaling of the spectral and steady-state quantities (say, X), the finite-size scaling of the boundaries of the multiple regimes (say, P, C, D) and the g_{eff} scaling of the quantities in the crossover regime (say, of X in C), respectively.

We define three regimes with N -dependant boundaries in which some quantity Q has qualitatively distinct behaviours: P_Q , for $g_{\text{eff}} \lesssim (\beta N)^{\kappa_Q^<}$; C_Q for $(\beta N)^{\kappa_Q^<} \lesssim g_{\text{eff}} \lesssim (\beta N)^{\kappa_Q^>}$; and D_Q for $(\beta N)^{\kappa_Q^>} \lesssim g_{\text{eff}}$. In P_Q , Q behaves as

$$Q \propto g_{\text{eff}}^2 (\beta N)^{\nu_Q^P} f_Q^<[(\beta N)^{-\kappa_Q^<} g_{\text{eff}}], \quad (\text{S1})$$

while in D_Q ,

$$Q \propto g_{\text{eff}}^2 (\beta N)^{\nu_Q^D} f_Q^>[(\beta N)^{-\kappa_Q^>} g_{\text{eff}}]. \quad (\text{S2})$$

Note that some extra factors of g_{eff} may exist (such as the extra g_{eff}^2 for X) but they do not modify the argument, as long as they are the same in regimes P_Q and D_Q . If they are different, a straightforward modification of Eq. (S5) below is required, but this issue did not arise for the quantities studied in this work. We further assume that the scaling functions f_Q have asymptotic power-law behaviours, that is, $f_Q^<(x) \propto x^0$ if $x \rightarrow 0$, $f_Q^<(x) \propto x^{\lambda_Q^<}$ if $x \rightarrow \infty$, $f_Q^>(x) \propto x^0$ if $x \rightarrow \infty$ and $f_Q^>(x) \propto x^{\lambda_Q^>}$ if $x \rightarrow 0$. The two limiting behaviours of Q should match in the intermediate regime C_Q , that is,

$$\begin{aligned} \lim_{g_{\text{eff}}(\beta N)^{-\kappa_Q^<} \rightarrow 0} (\beta N)^{\nu_Q^P} f_Q^<[(\beta N)^{-\kappa_Q^<} g_{\text{eff}}] &\simeq \\ \simeq \lim_{g_{\text{eff}}(\beta N)^{-\kappa_Q^>} \rightarrow \infty} (\beta N)^{\nu_Q^D} f_Q^>[(\beta N)^{-\kappa_Q^>} g_{\text{eff}}], & \quad (\text{S3}) \end{aligned}$$

whence the equality

$$g_{\text{eff}}^{2+\lambda_Q^<} (\beta N)^{\nu_Q^P - \kappa_Q^< \lambda_Q^<} = g_{\text{eff}}^{2+\lambda_Q^>} (\beta N)^{\nu_Q^D - \kappa_Q^> \lambda_Q^>} \quad (\text{S4})$$

follows. This equality implies that $\lambda_Q^< = \lambda_Q^> \equiv \lambda_Q$ and establishes a relation between ν , κ and λ exponents, which are thus not all independent but constrained by

$$\lambda_Q (\kappa_Q^> - \kappa_Q^<) = \nu_Q^D - \nu_Q^P. \quad (\text{S5})$$

Table S1 shows the values of the various exponents for $r = 1$ and $r > 1$, as defined above. It can be checked that all satisfy Eq. S5. Note that the exponent ν_Q^C (giving the collapse of curves of different βN in regime C_Q) is not defined in the above argument and thus does not enter the constraint. However for all cases of interest we either found $\nu_Q^C = \nu_Q^P$ or $\nu_Q^C = \nu_Q^D$.

S2. Global Spectrum

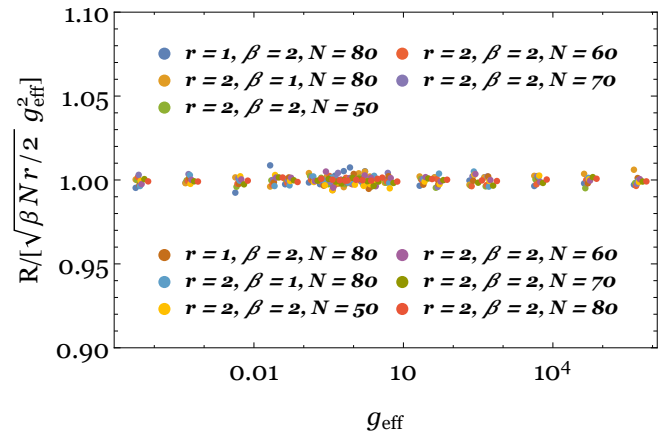


Figure S1. Center of mass R of the spectrum for different combinations of N , β , r and g .

The scaling of the spectrum in the various dissipation regimes can be motivated by the scaling of the two terms in Eq. (2). The spectral density of H is given by the Wigner semicircle law, with zero mean and width proportional to $\sqrt{\beta N}$. The dissipation matrix d is a Wishart matrix of rank- r , hence its spectral density follows the Marchenko-Pastur law, with mean $\propto \beta N r g^2$ and width $\propto \beta N \sqrt{r} g^2$. Since the eigenvalues of H and d are real, when considered separately, i.e. at the non-dissipative ($g = 0$) or at the fully dissipative ($g = \infty$) limits respectively, they only contribute to the imaginary or to the real parts of Λ , respectively. Although at finite g these considerations are no longer exact, we expect them to yield the leading scaling behaviour. Thus, only the dissipative term contributes to the mean of Λ and we have $R \propto \beta N r g^2$, see Fig. S1. For weak dissipation the Y scaling is dominated by the Hamiltonian term, hence

Table S1. Scaling exponents for $r = 1$ and $r > 1$, as defined in the main text. ν exponents give the finite-size scaling of the spectral and steady-state quantities within one of the regimes P, C, D and their primed counterparts; λ exponents give the extra g_{eff} -scaling besides g_{eff}^2 in regime C and its primed counterparts; κ exponents give the finite-size scaling of the boundaries of the regimes.

r	ν_P	ν_C	ν_D	λ_X	$\kappa_X^<$	$\kappa_X^>$	$\nu_{P'}$	$\nu_{C'}$	$\nu_{D'}$	λ_Δ	$\kappa_\Delta^<$	$\kappa_\Delta^>$	$\nu_{P''}$	$\nu_{C''}$	$\nu_{D''}$	λ_{ρ_0}	$\kappa_{\rho_0}^<$	$\kappa_{\rho_0}^>$
$= 1$	0	1/2	1/2	2	-1/4	0	1/2	1/2	-3/2	-8/3	0	3/4	-3	-2	-1	8/5	-1/2	3/4
> 1	0	1/2	1/2	2	-1/4	0	1/2	1/2	1/2	—	0	0	-3	-2	-2	2	-1/2	0

$Y \propto \sqrt{\beta N}$ (see Fig. 1 (e) in the main text). At large g the main contribution to X comes from the dissipative term and $X \propto \sqrt{\beta N} \sqrt{r} g^2$ (see Fig. 1 (d) in the main text). The passage from the weak dissipation scalings to the strong dissipation scalings should occur when the two terms in the Liouvillian are of the same order, $\sqrt{\beta N} \simeq \beta N \sqrt{r} g^2$, i.e. $g_{\text{eff}} \simeq 1$.

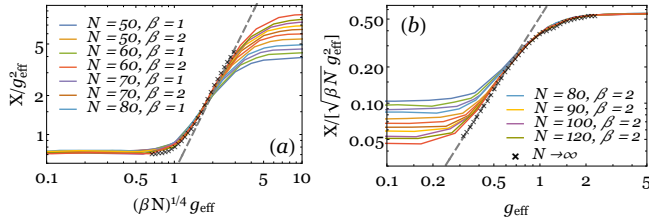


Figure S2. X as a function of g_{eff} for $r = 2$ and various N and β . The black crosses give the extrapolation of the data for $N \rightarrow \infty$ and the dashed gray line is $\propto g_{\text{eff}}^{\lambda_X}$. Collapse to the universal curve for small- g_{eff} in (a) and for large- g_{eff} in (b).

By fitting the global spectral data to power-laws, we find very good agreement with the exponents in Table S1. $\nu_C = \nu_D$ is completely independent of r . ν_P seems to decrease slightly with r , although the dependence is weak, and is most likely due to the reduced sizes possible to attain numerically. Furthermore, the exponents $\lambda_X = 2$ and $\kappa_X^< = -1/4$ are compatible with data extrapolation for $N \rightarrow \infty$, see Fig. S2. For both large- g_{eff} (Fig. S2 (a)) and small- g_{eff} (Fig. S2 (b)), the extrapolated data to $N \rightarrow \infty$ (black crosses), taken as the y -intercept of a linear fit in $(\beta N)^{-1}$, agrees very well with the power-law $g_{\text{eff}}^{\lambda_X}$ (gray line) in regime C. Upon entering regimes P and D, the extrapolation points naturally start deviating from the power-law curve.

S3. Spectral Gap

It is worth noting that fitting directly the numerical average spectral gap for several N and multiple $r > 1$ seems to indicate that there is a dependence of the scaling exponents $\nu_{P'}$, $\nu_{C'}$, $\nu_{D'}$ with r . In particular, $\nu_{P'} = \nu_{C'} = \nu_{D'}$ only for large r but $\nu_{P'} > \nu_{C'} > \nu_{D'}$ for small $r > 1$. However, this is incompatible with both the picture drawn in Sec. S1 and with the finiteness of

the gap in the thermodynamic limit for $r > 1$, discussed below. Since we can only access relatively small N , this apparent r -dependence is likely a finite-size effect suppressed by r . Indeed, values of the exponents obtained by data extrapolation to large N are compatible with $\nu_{P'} = \nu_{C'} = \nu_{D'} = 1/2$, independently of r .

For all regimes, the variance of the gap decreases with N and the value of Δ becomes sharply defined around its mean, see the gap distribution functions depicted in Fig. S3. The mean of the different distributions is not constant due to the finite-size effects discussed above.

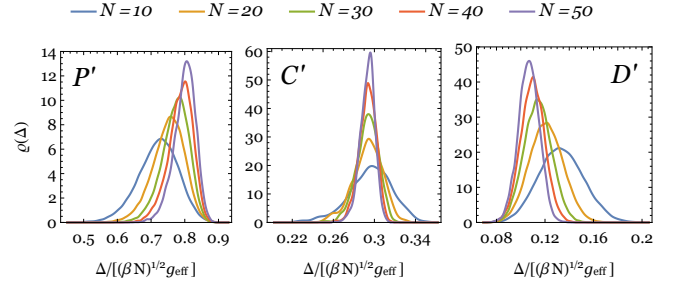


Figure S3. Scaled gap distribution function for each of the regimes P', C', D'.

We now provide the analysis yielding the results presented in the main text on the limiting behaviour of the spectral gap at small- and large- g_{eff} . For strong dissipation, we have $\mathcal{L} \simeq \sum_\ell \mathcal{D}_{W_\ell}$. The endpoints of the spectrum of \mathcal{L} along the real direction in the complex plane (that is, the spectral gap and left-most point of the lemon-shaped support, which is the gap plus some order-unity multiple of X) can be accessed directly by the use of the holomorphic Green's function of \mathcal{L} [21–23], $G = \text{Tr}\langle(z - \mathcal{L})^{-1}\rangle$. This was exploited in Ref. [17] to compute the spectral form factor. Note that, unfortunately, the information along the imaginary axis (for instance Y) and the spectral density inside the support cannot be accessed by this method.

When computing the holomorphic Green's function, it can be shown [17] that the terms $W_\ell \otimes W_\ell^*$ do not contribute in the large- N limit. For a single jump operator, the superoperator under consideration is then of the form $\mathcal{L} \simeq -\frac{1}{2}(\Gamma \otimes \mathbb{1} + \mathbb{1} \otimes \Gamma)$, where $\Gamma = W^\dagger W$ is a square Wishart matrix. Since the two sectors of the Liouvillian tensor product representation do not see each other, we can do independent expansions for each Wishart matrix.

Then, n^{th} -order terms of the expansion of the Liouvillian Green's function are given by all possible combinations of n_1^{th} -order terms of one of the Wishart matrices with all n_2^{th} -order terms of the other Wishart matrix, restricted by $n_1 + n_2 = n$ and there are $\binom{n}{n_1}$ such combinations for each fixed n . By summing all terms, the holomorphic Green's function of \mathcal{L} is then

$$G_{\mathcal{L}}(z) = \sum_{n=0}^{\infty} \frac{1}{z^{n+1}} \left(-\frac{1}{2}\right)^2 \sum_{k=0}^n \binom{n}{k} C_k C_{n-k}, \quad (\text{S6})$$

where C_k counts the number of Wishart planar diagrams at k^{th} order and is given by the Catalan numbers, whose real-integral representation is $C_n = (1/2\pi) \int_0^4 dx x^{n-1} \sqrt{4x-x^2}$, i.e. the moments of the Marchenko-Pastur distribution, $\varrho_{\text{MP}}(x) = \sqrt{x(4-x)}/(2\pi x)$, $0 < x < 4$. Inserting the integral representation of the Catalan numbers into Eq. (S6), performing the sum and comparing with the relation between the holomorphic Green's function and the spectral density $\varrho_{\mathcal{L}}$, $G_{\mathcal{L}}(z) = \int d\nu \varrho_{\mathcal{L}}(\nu)/(z-\nu)$, we arrive at

$$\varrho_{\mathcal{L}}(x) = 2 \int_{\nu_m}^{\nu_M} d\nu \varrho_{\text{MP}}(\nu) \varrho_{\text{MP}}(-\nu - 2x), \quad (\text{S7})$$

with $\nu_m = \max\{0, -2x - 4\}$ and $\nu_M = \min\{4, -2x\}$, whence it follows that $0 < x < 4$. Hence, the computation of the holomorphic Green's function has lead us to a convolution of two Marchenko-Pastur laws, which is the spectral density of half the sum of two uncorrelated Wishart matrices. Although the spectral density $\varrho_{\mathcal{L}}$ does not correctly describe the spectrum of the Liouvillian, it does predict its endpoints and the interval $[0, 4]$ in which $\text{Re}(\Lambda)$ is supported.

For more than one jump operator, Γ is a sum of r identical (i.e. independent but sampled from the same distribution) Wishart matrices. In Ref. [17] it was shown, using free-addition of random matrices, that the spectral density of Γ is again a Marchenko-Pastur distribution, but with endpoints dependent on r ,

$$\varrho_{\Gamma}(x) = \frac{1}{2\pi x} \sqrt{(\xi_+ - x)(x - \xi_-)}, \quad \xi_- < x < \xi_+, \quad (\text{S8})$$

where $\xi_{\pm} = (1 \pm \sqrt{r})^2$. But we have just seen that the computation of the spectral density from the holomorphic Green's function is equivalent to computing it for the half-sum of two uncorrelated matrices Γ , whence it immediately follows that \mathcal{L} is supported in $[-\xi_+, -\xi_-]$. We thus see, in agreement with Ref. [17], that $\langle \Delta \rangle = \beta N g^2 \xi_- = \sqrt{\beta N} g_{\text{eff}}^2 (1 - \sqrt{r})^2 / \sqrt{2r}$, while $X \propto \beta N g^2 (\xi_+ - \xi_-) \propto \sqrt{\beta N} g_{\text{eff}}^2$, with the proportionality constant of order unity, and where we have reintroduced the variances $\beta N g^2$. The latter result was already verified in the main text and motivated in an alternative way in the previous section.

The prediction for the gap at large g_{eff} for different r is depicted in Fig. S4, together with extrapolated data to

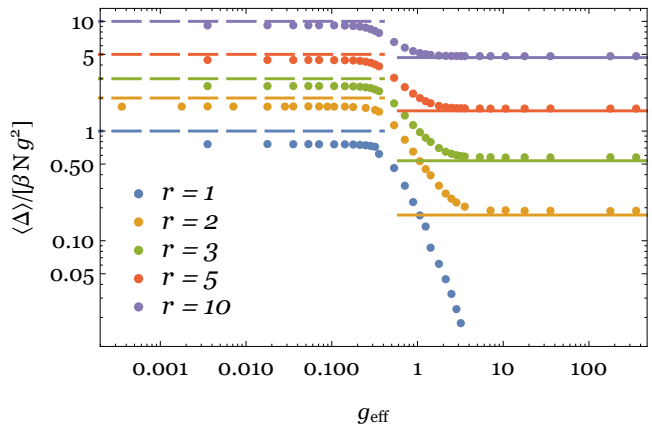


Figure S4. Evolution of the extrapolated spectral gap at $N \rightarrow \infty$ with g_{eff} for $r = 2, 3, 5$ and 10 . The dashed lines are the perturbative results $\langle \Delta \rangle = \beta N g^2 r$ for small g_{eff} , the full lines the analytic predictions $\langle \Delta \rangle = \beta N g^2 (1 - \sqrt{r})^2$ for large g_{eff} .

$N \rightarrow \infty$ for several values of r , and in Fig. 3 (main text) for r up to 60. We see that even at small r , the theoretical prediction correctly describes the spectral gap for a wide range of g_{eff} (that is, in the whole D' regime). Note also that $\langle \Delta \rangle \rightarrow 0$ at large g_{eff} for $r = 1$ in the thermodynamic limit, consistent with our results in Sec. S5.

For small g_{eff} , we can proceed perturbatively. If H is diagonal in the basis $|k\rangle$, $H = \sum_k \varepsilon_k |k\rangle \langle k|$, then the eigenstates of \mathcal{L} at $g = 0$ are $\rho_{kk'} = |k\rangle \langle k'|$ with eigenvalue $\Lambda_{kk'} = -i(\varepsilon_k - \varepsilon_{k'})$ ($k, k' = 1, \dots, N$). We thus have a N -fold degeneracy of stationary eigenstates, while the other eigenvalues form $N(N-1)/2$ complex conjugate pairs. Any amount of dissipation lifts the degeneracy of the zero-eigenvalue subspace but for small enough dissipation the two sectors will not mix and we expect that the long-time dynamics (the gap) and the (now unique) steady-state are determined from the states in the (previously-) degenerate subspace. We lift the degeneracy by diagonalizing the perturbation $\sum_{\ell} \mathcal{D}_{W_{\ell}}$ in that subspace and we obtain the eigenvalues of \mathcal{L} to first order,

$$\begin{aligned} A_{nm} &\equiv \langle \langle nn | \sum_{\ell} \mathcal{D}_{W_{\ell}} | | mm \rangle \rangle \\ &= \begin{cases} \sum_{\ell} W_{nm}^{(\ell)} W_{nm}^{(\ell)*}, & \text{if } m \neq n, \\ -\sum_{\ell} \sum_{k \neq m} W_{km}^{(\ell)} W_{km}^{(\ell)*}, & \text{if } m = n, \end{cases} \end{aligned} \quad (\text{S9})$$

with the superoperator notation $| | mn \rangle \rangle = |m\rangle \otimes \langle n|^{\text{T}}$.

From Eq. (S9) it follows that

$$A_{nm} \in \mathbb{R} \quad (\text{for all } n), \quad (\text{S10a})$$

$$A_{nm} > 0 \quad (n \neq m), \quad (\text{S10b})$$

$$\sum_{n=1}^N A_{nm} = 0 \quad (\text{for all } n), \quad (\text{S10c})$$

which are the conditions for A to be the generator of a classical stochastic equation [15, 19], $\partial_t \mathbf{P} = A\mathbf{P}$, where \mathbf{P} is a probability vector. The diagonal entries $A_{mm} = -\sum_{k \neq m} A_{km}$ are determined by the off-diagonal entries, hence we must only determine the distribution of the latter. For $n \neq m$, the distribution of the entry A_{nm} depends on the nature of the jump operator as follows. $W_{nm}^{(\ell)}$ is a Gaussian random variable with variance σ^2 with β real degrees of freedom. Then $A_{nm} = \sum_{\ell} W_{nm}^{(\ell)*} W_{nm}^{(\ell)} = \sum_{\ell} |W_{nm}^{(\ell)}|^2$ is (in terms of real degrees of freedom) a sum of $r\beta$ squared Gaussian iid variables and hence follows a χ^2 -distribution with $k = r\beta$ degrees of freedom. The distribution function of the entries A_{nm} is

$$P_k(A_{nm}) = \frac{(A_{nm})^{\frac{k}{2}-1} \exp -\frac{A_{nm}}{2\sigma^2}}{(2\sigma^2)^{\frac{k}{2}} \Gamma(\frac{k}{2})}. \quad (\text{S11})$$

Ensembles of real exponential distributed matrices (corresponding to $k = 2$) with the diagonal constraint (S10c) were studied in Refs. [19]. In particular, it was shown that, in the large N -limit the spectral density depends only on the second moment of the distribution, $\tau_k^2 \equiv \langle A_{nm}^2 \rangle - \langle A_{nm} \rangle^2 = 2k\sigma^4$, and can therefore be calculated from any distribution of entries having this variance, particularly for a Gaussian distribution, which was done in Ref. [24] for symmetric A . Furthermore, in Ref. [19] it was numerically found that the average smallest nonzero eigenvalue of A (the symmetric value of the spectral gap here) is $N\langle R \rangle$ for large N , where $\langle R \rangle$ is the mean of the exponential ($k = 2$) distribution of A_{nm} . Generalizing to the general χ^2 -distribution, with mean $\mu_k = k\sigma^2$, we find that $\langle \Delta \rangle = \beta N r g^2 = \sqrt{\beta N r / 2} g_{\text{eff}}$. The comparison of this result with numerical data for the average spectral gap for various r is given in Fig. S4 as a function of g_{eff} and for extrapolated $N \rightarrow \infty$ and in Fig. 3 (main text) for r up to $r = 60$ for fixed $N = 60$ and two fixed g (one for strong dissipation, one for weak). We see that although there is some deviation from the theoretical curves at small r , they describe the numerical data increasingly well with growing r .

Finally, we note that the exponent λ_{Δ} is not defined. The arguments of Sec. S1 do not provide the value of λ_{Δ} since $\nu_P' = \nu_D'$ and $\kappa_{\Delta}^< = \kappa_{\Delta}^>$. This stems from the fact that for the gap, different scaling functions for small and large dissipation, which asymptotically match in an intermediate region of size growing with N , do not exist. Instead, the gap is described by a single scaling function for all N .

S4. Steady-state

Next, we analyse the steady-state properties for $r > 1$. The finite-size scaling exponents $\nu_{P''} = -3$ and $\nu_{C''} = \nu_{D''} = -2$ are in very good agreement with fits of the

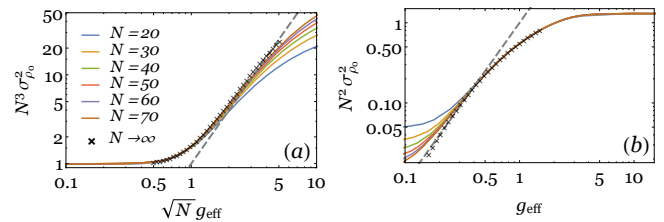


Figure S5. $\sigma_{\rho_0}^2$ as a function of g_{eff} for $r = 2$ and various N . The black crosses give the extrapolation of the data for $N \rightarrow \infty$ and the dashed gray line is $\propto g_{\text{eff}}^{\lambda_{\rho_0}}$. Note data collapse to the universal curve for small- g_{eff} in (a) and for large- g_{eff} in (b).

data to the respective power-laws, for various $r > 1$ ($r = 2, 3, 5, 10$) and show no dependence on r as expected. The exponents λ_{ρ_0} and $\kappa_{\rho_0}^<$ are also compatible with data extrapolation, see Fig. S5, by proceeding in the same way as for X .

S5. Spectral and steady-state properties for $r = 1$

For weak dissipation, the spectral and steady-state properties do not differ qualitatively between $r = 1$ and $r > 1$. In fact, in regime P'' the exponents are always the same in both cases. However, there are important differences at large g_{eff} for the spectral gap and the steady-state.

As was seen in Sec. S3, the spectral gap closes in the thermodynamic limit for $r = 1$. This can be seen immediately from the inversion of the sign of $\nu_{D'}$ and also from Fig. S6, where we plot the evolution of $\langle \Delta \rangle$ as a function of g_{eff} . For finite N , the gap does not close but settles instead to value $\propto g_{\text{eff}}^2$, with finite-size power-law $N^{-3/2}$.

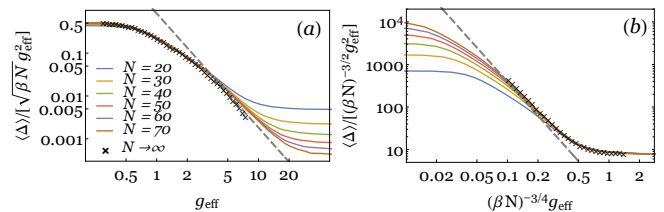


Figure S6. Average spectral gap as a function of g_{eff} for $r = 1$ and various N . The black crosses give the extrapolation of the data for $N \rightarrow \infty$ and the dashed gray line is $\propto g_{\text{eff}}^{\lambda_{\Delta}}$. Collapse to the universal curve for small- g_{eff} in (a) and for large- g_{eff} in (b).

For the $r = 1$ case, contrary to $r > 1$, the values of g_{eff} that define the boundaries between different regimes are N dependant. Hence a λ_{Δ} can be defined, for $r = 1$. The gap has a nonzero exponent $\kappa_{\Delta}^>$ and the matching procedure of Sec. S1 is applicable.

In particular, with $\kappa_{\Delta}^> = 3/4$ (see Fig. S6 (b)), we can use Eq. (S5) to determine $\lambda_{\Delta} = -8/3$. Furthermore, the

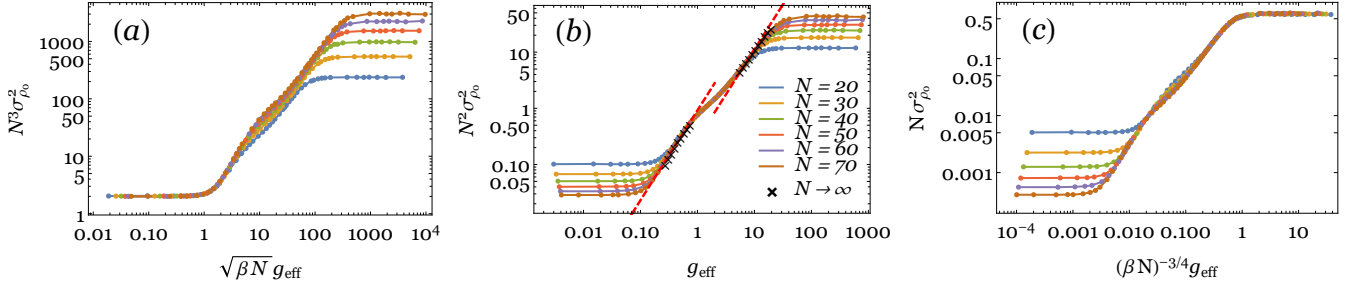


Figure S7. Variance of steady-state probabilities as a function of g_{eff} plotted for a single decay channel ($r = 1$), different values of N and $\beta = 2$. The rescalings of $\sigma_{\rho_0}^2$ and of g_{eff} are those so as to collapse the different curves to a single curve in the (a) P'' regime, (b) C'' regime, and (c) D'' regime. The dashed lines in (b) are obtained by fitting extrapolated data for $N \rightarrow \infty$ (black crosses) to power-law behaviour $g_{\text{eff}}^{\lambda_{\rho_0}}$ near the boundaries of regime C''.

exponents listed in Table S1 are compatible with data extrapolation, see Fig. S6. The procedure for data extrapolation is the same as before. However, given the small sizes available, as well as reduced statistics (each diagonalization yields only one value of the gap), we cannot exclude other similar exponents consistent with data extrapolation and which satisfy Eq. (S5).

Regarding the steady-state at large dissipation and $r = 1$, in Fig. S7 we show the evolution of the variance of steady-state eigenvalues as a function of g_{eff} . For $r = 1$ the condition $\nu_{C''} = \nu_{D''}$ is no longer verified, instead $\nu_{C''} = -2$. Using the values of $\nu_{P''}$ and $\kappa_{\rho_0}^<$ obtained from Fig. S7 (a), and of $\nu_{D''}$ and $\kappa_{\rho_0}^>$ obtained from Fig. S7 (c), Eq. (S5) gives the value $\lambda_{\rho_0} = 8/5$. Note

that in this case, both boundaries of regime C'' scale with N and the scaling function does have a single power-law behaviour throughout the intermediate regime. However, the power-law $g_{\text{eff}}^{\lambda_{\rho_0}}$ describes accurately the behaviour of $\sigma_{\rho_0}^2$ both when entering regime C'' from regime P'' and when entering regime C'' from regime D'', see the dashed lines in Fig. S7 (b). The two power-laws are shifted with respect to each other and are linked by a crossover region the center of regime C''.

Furthermore, we have $\sigma_{\rho_0}^2 \propto 1/N$ for strong dissipation, which gives a purity $\mathcal{P}_0 \propto N^0$ in the large- N limit. Thus, contrarily to the $r > 1$ case, the steady-state's purity is not proportional to that of the maximally mixed state but remains finite for large N .